Silicon (2021) 13:4737–4745
https://doi.org/10.1007/s12633-020-00788-5

ORIGINAL PAPER

Novel Design for the Temperature Sensing Using Annular Photonic Crystals

Mazen M. Abadla[1] · Hussein A. Elsayed[2] · Ahmed Mehaney[2]

Received: 28 August 2020 / Accepted: 14 October 2020 / Published online: 26 October 2020

Abstract

In this research, a high-performance temperature sensor of a one-dimensional defective annular photonic crystal is proposed. The structure design of our proposed defective annular photonic crystal is: $[(Si/SiO_2)^{N/2}\ TiO_2\ (Si/SiO_2)^{N/2}]$ with TiO_2 as a defect layer. The transmission spectrum of the defective annular photonic crystal is calculated by using the well-modified transfer matrix method in cylindrical coordinates. Thermal characteristics of the defect mode that emerged in the transmission spectrum are studied in the visible region. Dependence of the defect mode frequency on the defect layer thickness is also discussed. As temperature increases, the defect mode is shifted to new positions due to thermal expansion and thermo–optical effects. Numerical results show that the core radius has an important effect on the transmission intensity of the defect mode. Moreover, our proposed temperature sensor showed a sensitivity of about 11 nm / 1000 °C, figure of merit of 0.218 / °C and a very small full width at half maximum of about 0.049 nm. The proposed annular photonic crystals temperature sensor could present a novel method to overcome the limited performance of the planar photonic crystals temperature sensors besides the possibility of using in many potential filtering applications.

Keywords Annular photonic crystals · Thermo-optics effect · Temperature sensor · Defect mode · Photonic band gaps

1 Introduction

Photonic crystals (PCs) could be designed in one, two, and three dimensions from periodic arrangements of materials reliance on the refractive indices periodicity of these materials [1–4]. Among the past three decades, these structures have been widely attracting a large area of interest through many scientific circles due to their contributions in many applications [5–8]. These applications experienced a remarkable increase since the discovery of the photonic band gaps (PBGs) by Yablonovitch and the photon localization by John [9, 10].

Compared with the two, and three dimensional PCs, the one-dimensional PCs represent the simplest type of PCs from the design and fabrication view. Therefore, it acquires significant popularity among the physical, biomedical and optical communities. The one dimensional PCs became prominent in many applications such as optical filters [11], switches [12], modulators [13, 14] and sensors [15–20]. These great number of applications devoted the researchers toward the inclusion of the one dimensional PCs in new designs such as quasi-crystal PCs [1] and new geometries such as annular PCs [21–23]. This diversity was intended to improve the optical properties and extinguish more facilities in fabrications of the one dimensional PCs.

The annular photonic crystals (APCs) that are also known as cylindrical PCs received considerable attention due to the remarkable improvements in the theoretical models and the fabrication techniques [3, 8]. Recently, one dimensional APCs have been designed using different types of materials for many applications. Kaliteevski et al. [22] discussed the reflectance properties of the APCs using dielectric materials. Hu et al. investigated the role played with the liquid crystals in the design of an optical switch using the APCs [24]. Such a study indicates the enhancement in the reflectance characteristics compared with the traditional PCs. Moreover, this study is much more suitable from the fabrication view, particularly in the case of using

✉ Hussein A. Elsayed
drhussien85sc@gmail.com;
hussien.abdelghani@science.bsu.edu.eg

[1] Physics Department, Faculty of Science, Al-Aqsa University, Palestinian Authority, Gaza City, Palestine

[2] TH-PPM Group, Physics Department, Faculty of Science, Beni-Suef University, Beni Suef, Egypt

liquids as a defect, for the detection and sensing applications. Thus, this new geometry could increase the possibility of using the one dimensional PCs in the biomedical and engineering applications. Further works demonstrated the optical characteristics of APCs using dielectrics, metals, superconductors and metamaterials [21, 25–27].

The design of temperature sensors using PCs provides low sensitivity especially for using solid materials. For example, Chang et al. designed a temperature sensor in the visible light using the one dimensional defective PCs [28]. However, this sensor investigates a low value of sensitivity not exceeding 0.005 nm / °C. To the best of our knowledge, the temperature sensing using the APCs has not yet received the desired attention in contemporary times.

Here, we demonstrate theoretically the design of a temperature sensor using the APCs that contain a defect layer. The refractive index of the defect layer varies with the temperature change so that the properties of the defect mode could be controlled with temperature. Our idea is essentially based on the enhancement of the sensitivity of our temperature sensor in comparison to its counterparts in the planar PCs. The interaction of the incident electromagnetic waves with our design can be theoretically described using the well modified transfer matrix method. This method is used to obtain the optical characteristics of our design due to this interaction. Here, we intend to discuss the effect of the defect layer thickness, the number of periods and the radius of the core on the performance of our sensor.

When the core radius is large enough compared with the layers' thicknesses, the situation is more likely to be a planar structure with normal incident radiation [29]. This is an advantage over the conventional planar waveguide sensors in which the angle may result in unwanted fake results. This gives additional flexibility in positioning the sensing probe equally anywhere on the rim of the outermost concave surface. This advantage cannot be achieved in planar PCs where the probe is located only at a planar (not round) surface. A third important advantage of adopting APCs arises from the exhibition of considerable higher sensitivity and performance factors.

In what follows, we present the basics features of the well modified transfer matrix method in section 2. Then, in section 3, we present the transmittance properties of our design besides the discussions of the values of many parameters such as the sensitivity, detection limit, signal to noise ratio and the sensor resolution. Finally, section 4 describes a brief summary of the results and output findings.

2 Theoretical Framework

A schematic representation of the sensor under consideration is shown in fig. 1. A core of radius ρ_o and refractive index n_0 is covered with periodic two-alternative layers of thicknesses h_1 and h_2 and refractive indices n_1 and n_2; respectively. A defect layer of thickness h_d is located a distance $\rho_o + \frac{N}{2}\Lambda$ such that $\Lambda = h_1 + h_2$ is the period and N is an even number of periods so that our structure is $(AB)^{N/2}$ D $(AB)^{N/2}$. All constituents are assumed to be nonmagnetic so that: $\mu = \mu_r \mu_0 = \mu_0$. In addition, these layers are temperature dependent in such a way that refractive indices and radii can be expressed as [28, 30]:

$$n_j = n_j^{(0)} + \beta_j \Delta T \tag{1a}$$

$$\rho_j = \rho_j^{(0)}\left(1 + \alpha_j \Delta T\right) \tag{1b}$$

such that: $j = 0, 1, 2$, ΔT is the temperature change, $n_j^{(0)}$ and $\rho_j^{(0)}$ are the refractive indices and radii at room temperature, respectively. Here, α_j is the coefficient of thermal expansion and β_j is the thermo-optic coefficient of the j^{th} medium.

To analyze the problem, cylindrical waves (with $e^{-i\omega t}$ dependence) are assumed to propagate within the fiber layers from the core towards the outer layers. Adopting cylindrical coordinate system, the fields (E_z, H_ϕ,, H_ρ) of the TE polarization (the E-type mode) satisfy the Helmholtz equation given as [30–32]:

$$\frac{1}{\rho}\frac{\partial}{\partial \rho}\left(\rho \frac{\partial E_z}{\partial \rho}\right) + \frac{1}{\rho^2}\frac{\partial^2 E_z}{\partial \phi^2} + \varepsilon_o \mu_o \varepsilon \mu \omega^2 E_z = 0 \tag{2}$$

Expressing E_z as: $E_z = F(\rho)\, \Phi(\phi)$, Eq. (2) can be solved to give [24, 33, 34]:

$$E_z(\rho, \phi, z) = [A J_\nu(q\rho) + B Y_\nu(q\rho)]\exp(i\nu\phi) \tag{3}$$

where, J_ν and Y_ν are the Bessel functions of the first and second kinds, respectively, $q_j^2 = \varepsilon_o \varepsilon \mu_o \omega^2 = k_o^2 n_j^2$ is the propagation constant and ν is the azimuthal number. Accordingly; the tangential component of the magnetic field H_ϕ is given by:

$$H_\phi = \frac{i}{\omega \mu_o}\frac{\partial E_z}{\partial \rho} = \frac{i}{\omega \mu_o}\left[A J_\nu'(q\rho) + B Y_\nu'(q\rho)\right]\exp(i\nu\phi) \tag{4}$$

In our discussion, we are concerned in the transmittance outward of the structure so that, and without any loss of generality, the azimuthal number has been set to zero so that the fundamental mode is considered. This give rise to:

$$E_z = A J_0(q\rho) + B Y_0(q\rho) \tag{5a}$$

$$H_\phi = -\frac{iq}{\omega \mu_o}[A J_1(q\rho) + B Y_1(q\rho)] \tag{5b}$$

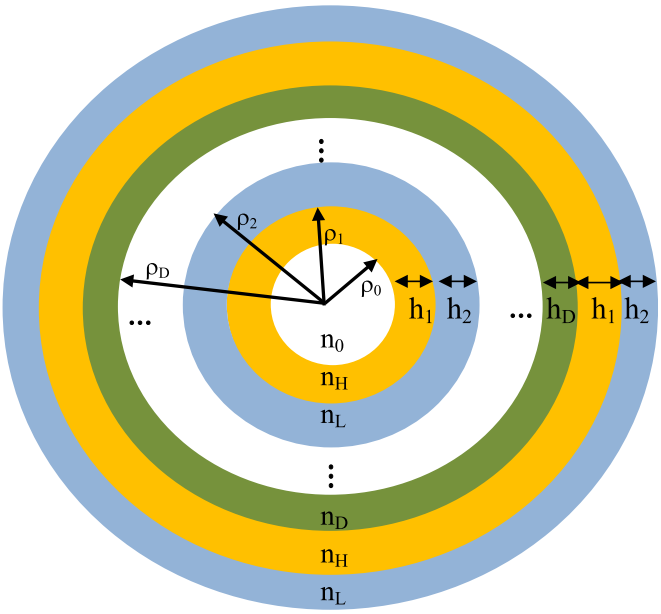

Fig. 1 A schematic diagram of the one dimensional defective APCs in which two different materials of refraction indices: n_1 and n_2 and thicknesses: h_1 and h_2. The defect layer has a refractive index n_D and thickness h_D.

These fields can be put in a matrix form as:

$$\begin{pmatrix} E_z \\ H_\phi \end{pmatrix} = \begin{pmatrix} J_0(q\rho) & Y_0(q\rho) \\ -\frac{iq}{\omega\mu_o} J_1(q\rho) & -\frac{iq}{\omega\mu_o} Y_1(q\rho) \end{pmatrix} \begin{pmatrix} A \\ B \end{pmatrix} \tag{6}$$

Consequently; the amplitudes A and B are given as:

$$\begin{pmatrix} A \\ B \end{pmatrix} = \begin{pmatrix} J_0(q\rho) & Y_0(q\rho) \\ -\frac{iq}{\omega\mu_o} J_1(q\rho) & -\frac{iq}{\omega\mu_o} Y_1(q\rho) \end{pmatrix}^{-1} \begin{pmatrix} E_z \\ H_\phi \end{pmatrix} \tag{7}$$

Matching the fields at the interface $\rho = \rho_0$ then:

$$\begin{pmatrix} E_0 \\ H_0 \end{pmatrix}_{\rho=\rho_0} = \begin{pmatrix} E_1 \\ H_1 \end{pmatrix}_{\rho=\rho_0} = \begin{pmatrix} J_0(q_1\rho_0) & Y_0(q_1\rho_0) \\ -\frac{iq_1}{\omega\mu_o} J_1(q_1\rho_0) & -\frac{iq_1}{\omega\mu_o} Y_1(q_1\rho_0) \end{pmatrix} \begin{pmatrix} A_1 \\ B_1 \end{pmatrix} \tag{8}$$

Since A's and B's are invariant within the same layer, then:

$$\begin{pmatrix} A_1 \\ B_1 \end{pmatrix} = \begin{pmatrix} J_0(q_1\rho_1) & Y_0(q_1\rho_1) \\ -\frac{iq_1}{\omega\mu_o} J_1(q_1\rho_1) & -\frac{iq_1}{\omega\mu_o} Y_1(q_1\rho_1) \end{pmatrix}^{-1} \begin{pmatrix} E_2 \\ H_2 \end{pmatrix}_{\rho=\rho_1} \tag{9}$$

Substituting from Eq. (9) into Eq. (8), then the fields at the first and second interfaces can be related through a transfer matrix $\mathbf{T}_1$ as:

$$\begin{pmatrix} E_0 \\ H_0 \end{pmatrix}_{\rho=\rho_0} = T_1 \begin{pmatrix} E_2 \\ H_2 \end{pmatrix}_{\rho=\rho_1} \tag{10}$$

The transfer matrix $\mathbf{T}_1$ is expressed as:

$$T_1 = \begin{pmatrix} J_0(q_1\rho_0) & Y_0(q_1\rho_0) \\ -\frac{iq_1}{\omega\mu_o} J_1(q_1\rho_0) & -\frac{iq_1}{\omega\mu_o} Y_1(q_1\rho_0) \end{pmatrix} \begin{pmatrix} J_0(q_1\rho_1) & Y_0(q_1\rho_1) \\ -\frac{iq_1}{\omega\mu_o} J_1(q_1\rho_1) & -\frac{iq_1}{\omega\mu_o} Y_1(q_1\rho_1) \end{pmatrix}^{-1} \tag{11}$$

Following up the same approach, the fields at the first and last interfaces are related through an overall transfer matrix as:

$$\begin{pmatrix} E_0 \\ H_0 \end{pmatrix}_{\rho=\rho_0} = T_1 T_2 T_3 \ldots T_{N/2} T_D T_{N/2+1} \ldots T_{N-2} T_{N-1} T_N \begin{pmatrix} E_f \\ H_f \end{pmatrix}_{\rho=\rho_N} = m \begin{pmatrix} E_f \\ H_f \end{pmatrix}_{\rho=\rho_N} \tag{12}$$

where, **m** is the overall transfer matrix. The fields within a layer can be expressed as a linear combination of diverging and converging fields as [30, 32, 33]:

$$E_z = A_1 H_0^{(1)}(q\rho) + A_2 H_0^{(2)}(q\rho)\Big] = E^+ + E^- \tag{13}$$

such that; $H_0^{(1,2)}(q\rho)$ are the Hankel functions given by:

$$H_0^{(1,2)}(q\rho) = J_0(q\rho) \pm i\, Y_0(q\rho) \tag{14}$$

Here, the + and – signs denote the diverging ($H^{(1)}$) and converging ($H^{(2)}$) fields; respectively. Accordingly; the magnetic field H_ϕ can be written as:

$$H_\varnothing = \frac{i}{\omega\mu_o}\frac{\partial E_z}{\partial\rho} = -\frac{iq}{\omega\mu_o}\left[C_0^{(1)}E^+ + C_0^{(2)}E^-\right] \tag{15}$$

where: $C_0^{(1,2)} = \frac{J_1(q\ \rho)\pm iY_1(q\ \rho)}{J_0(q\ \rho)\pm iY_0(q\ \rho)}$

In matrix form, one may write the tangential fields as:

$$\begin{pmatrix} E_z \\ H_\phi \end{pmatrix} = \begin{pmatrix} 1 & 1 \\ -\frac{iq}{\omega\mu_o}C_0^{(1)}(q\rho) & -\frac{iq}{\omega\mu_o}C_0^{(2)}(q\rho) \end{pmatrix}\begin{pmatrix} E^+ \\ E^- \end{pmatrix} = W\begin{pmatrix} E^+ \\ E^- \end{pmatrix} \tag{16}$$

Substituting from Eq. (16) into Eq. (11) and arranging, then:

$$\begin{pmatrix} 1 \\ r \end{pmatrix}_{\rho=\rho_0} = W_0^{-1}mW_f\begin{pmatrix} t \\ 0 \end{pmatrix}_{\rho=\rho_f} = M\begin{pmatrix} t \\ 0 \end{pmatrix}_{\rho=\rho_f} \tag{17}$$

such that; r and t are the well-known Fresnel coefficients. The Fresnel transmission coefficient t is found from the transfer matrix **M** as:

$$t = \frac{1}{M_{11}} = \frac{-\left[C_\nu^{(1)}(q_0\rho_0) - C_\nu^{(2)}(q_0\rho_0)\right]}{C_\nu^{(2)}(q_0\rho_0)\left[m_{11} + iC_\nu^{(1)}\left(q_f\rho_f m_{12}\right] + \omega\mu_o\left[im_{21} - C_\nu^{(1)}\left(q_f\rho_f\right)m_{22}\right]} \tag{18}$$

Consequently; the transmittance T is calculated:

$$T = tt^* = \frac{1}{|M_{11}|^2} \tag{19}$$

3 Numerical Results and Discussion

3.1 Structure design

In this section, we discuss the thermal properties of the one dimensional defective APCs and study their performance with many parameters such as the defect layer thickness, core radius and specifically temperature changes.

The proposed APCs are suitable for designing sensors dealing with liquids in particular because the analyte is used to fill the tubes without running off the sensor. In biomedical sensing, the sensor may just be immersed in the analyte when it fills the appropriate region (defect area or repeated layers) and the sensing process takes place.

The transmittance properties of the APCs are calculated on basis of the theoretical analysis presented in the previous section. First, the proposed APCs structure containing N periods of alternate layers of Si and SiO_2 i.e. $(Si / SiO_2)^N$, is considered. Then, a defect layer of TiO_2 is supposed to be inserted in the middle of the perfect periodic APCs. The APCs are supposed to be immersed in air i.e. $n_0 = 1$. Here, the transmittance characteristics of the proposed APCs are calculated in the visible region. The initial values at 25°C for refractive index, thickness, thermo-optic coefficient and coefficient of thermal expansion of the constituents is given in table 1 below.

The refractive index of Si is described using Sellmeier formula as [35]:

$$n_{Si} = \sqrt{1 + \frac{10.6684293\ \lambda^2}{\lambda^2 - 0.0909} + \frac{0.00343474\ 84\ \lambda^2}{\lambda^2 - 1.2877} + \frac{1.54133408\ \lambda^2}{\lambda^2 - 1218816}} \tag{20}$$

where, λ is the wavelength of the incident electromagnetic waves.

Unlike the usual planar PCs, the core radius of the starting medium ρ_0 has an effective role in wave characteristics and on PBGs. With a large magnitude of the core radius, the cylindrical layers behave as if being planar. For this purpose the starting radius, otherwise mentioned is taken to equal 100-period length [29]. Moreover, the periods' number is chosen to be $N = 10$ giving rise to defective APCs of the configuration $[(Si / SiO_2)^5\ TiO_2\ (Si / SiO_2)^5]$. Because the constituent materials are considered as dielectric layers, the thermal properties of the proposed APCs will be described by the thermo-optic and thermal expansion effects.

3.2 Numerical Results

In what follows, we will discuss the numerical results of the defect mode dependence on temperature in a defective APCs. We first investigate the difference between the transmission spectra of perfect ordered and defective APCs. Figure 2 presents the transmittance of the incident electromagnetic waves of two APCs structures, $(Si / SiO_2)^{10}$ and $[(Si / SiO_2)^5\ TiO_2\ (Si / SiO_2)^5]$ at room temperature (T = 25 °C). In Fig. 2 (a), for the perfect ordered APCs, there is a wide PBG at the visible light region in the wavelength range 440 nm − 720 nm. The width of the PBG in the transmission spectrum of the defective APCs is almost unchanged as seen in Fig. 2(b). Also, it can be seen that there is a transmitted peak produced within the PBG at the wavelength value $\lambda_f = 550$ nm and with an intensity of about 53%. This transmittance peak is called a defect mode or resonant mode. The wavelength and intensity of this peak is related to the optical properties of the TiO_2 defect layer. The defective APCs act as a sub-diffractive regime or a narrowband filter for the incident electromagnetic waves which is well-known as Fabry–Perot resonator [28, 39].

Table 1 Parameters of the constituent materials of the proposed structure at room temperature [5,28, 36–38]

Materials	Refractive index	Thickness (nm)	Thermo-optic coefficient ($^oC^{-1}$)	Coefficient of therm. Expansion ($^oC^{-1}$)
Air	1	clad	1×10^{-6}	clad
Silicon (Si)	3.49	39.4	1.86×10^{-4}	5×10^{-7}
Silica (SiO_2)	1.45	94.8	1×10^{-5}	5.5×10^{-7}
Titania (TiO_2)	2.2	62.5	-2.3×10^{-5}	8×10^{-7}

Also, as seen in this figure, our defective APCs produce a sharp defect mode with a high Q- factor.

In Fig. 3, the effect of temperature on the defect mode of the defective APCs $[(Si / SiO_2)^5\ TiO_2\ (Si / SiO_2)^5]$ TiO_2 as a defect layer is carried out. In Fig. 3 (a), the thickness of the TiO_2 is taken as the previous quarter wavelength value and in Fig.3 (b) the thickness of the TiO_2 is increased to about a doubled value d_{TiO_2} = 120 nm. Fig. 3 (a) ascertains that temperature changes have a remarkable influence on the position of the defect mode. As the temperature increases over the room temperature, the defect mode is gradually shifted towards the longer wavelength regions till reaching the wavelength value 560.7 nm for $\Delta T = 1000$ °C. We could obtain a significant displacement in the position of the defect mode of about 11 nm and 18 nm for a temperature change of 1000 °C in Figs. 3(a) and Fig. 3(b), respectively. Thus, our defective APCs has high sensitivity compared with the conventional planar defective sensors [28, 40]. For example, in reference [28] Chang et al. obtained a sensitivity value of just 5 nm for temperature changes of the value 1000 °C. These results could be of interest for temperature sensors based on PC structures and especially it can work as a narrowband filter for monochromatic light in the presence of temperature effects. Wherein, we can obtain here a specified color at a certain temperature in the visible wavelength regions. The explanation of the defect mode dependence on temperature emerges from two factors effect simultaneously on the defect mode wavelength. The first parameter is the thermal expansion effect which makes the thickness of the defect layer and the temperature dependent constituent materials. The second factor is the thermo–optical effect, which causes the refractive index to increase with temperature.

In Fig. 4 (a) and (b), the resonance location in the $[(Si / SiO_2)^5\ TiO_2\ (Si / SiO_2)^5]$ APCs is plotted versus the (defect layer thickness) and (temperature changes), respectively. From Fig. 4 (a), it is obvious that choosing the defect layer of TiO_2 with higher thickness would increase the resonant wavelength of the defect mode. Here, the resonance location increases with temperature changes as depicted in Fig. 4 (b) for three defect layer thicknesses. The slopes of the lines in Fig. 4 (b) represent the sensitivity of the defective APCs. Wherein, as seen from this figure, sensitivity increases with temperature increase and it is highest for the defect layer thickness d_{TiO_2} = 120 nm. We did not plot the resonance location for a defect layer thickness of more than 120 nm in order not to exceed the visible region. This value at 120 nm is the maximum available thickness that maintains the visible spectrum. After that, infrared would work.

Unlike the usual planar PCs, the starting radius ρ_0 of the APCs plays an effective role in the PBG formation and defect mode properties. In Fig. 5, the maximum achievable transmittance of the defective APCs $[(Si / SiO_2)^5\ TiO_2\ (Si / SiO_2)^5]$ is plotted against the core radius (normalized to the period Λ) for $\Delta T = 0$ °C (red) and $\Delta T = 1000$ °C (blue). It is clear that the maximum transmittance in the defective APCs is achieved with a higher core radius. Such maximum transmittance

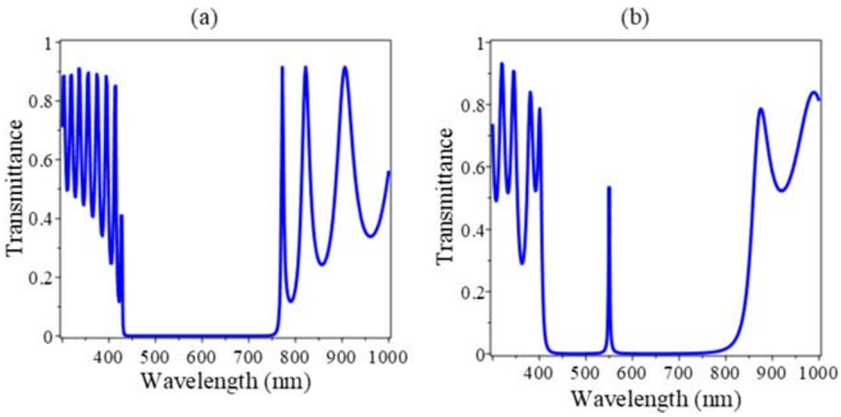

Fig. 2 The transmission spectra for two APCs structures of at room temperature, (a) $(Si/SiO_2)^{10}$ without defects and (b) $[(Si/SiO_2)^5\ TiO_2\ (Si/SiO_2)^5]$ with TiO_2 as a defect layer.

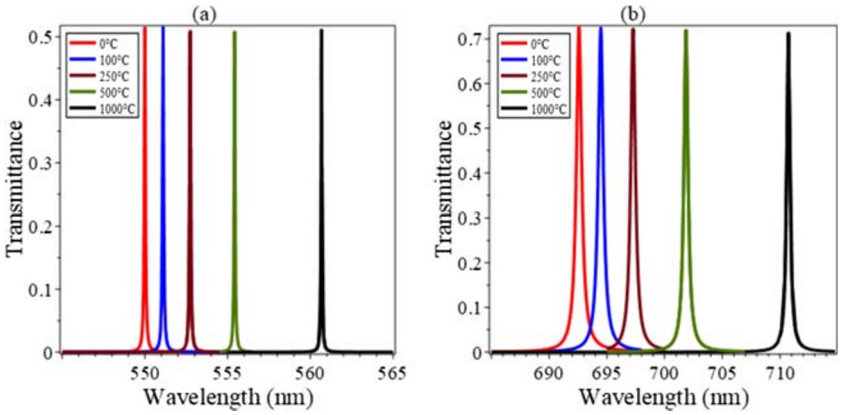

Fig. 3 The effect of temperature on the defect mode of $[(Si/SiO_2)^5\ TiO_2\ (Si/SiO_2)^5]$ at different temperatures. (a) d_{TiO_2} = 62.5 nm, (b) d_{TiO_2} = 120 nm and ΔT = 0 °C corresponds to the room temperature T = 25 °C.

increases with increasing temperature (blue line), which is considered as another confirmation of the last results of temperature effects on the defective APCs. When the starting radius is increased as temperature increases over the room temperature, the value of the transmitted defect mode increases as well. Such increase in the value of the maximum transmittance of the defect mode could be due to the change in the thickness and the index of refraction of the constituent materials with temperature.

3.3 Structure Performance

For the sensing process to occur, it is simply that the core is axially illuminated and a probe somewhere on the outermost cladding receives the transmitted radiation with the advantage that the radiation is considered as being normally incident to the layers. The performance of the defective APCs (as a sensor) is determined using specific parameters such as sensitivity (S), detection limit (δn), sensor resolution (SR), the figure of merit (FOM) and signal-to-noise ratio (SNR) [4, 41]. The sensitivity is given by

$$S = \frac{\Delta\lambda_{res}}{\Delta T} \tag{21}$$

where, $\Delta\lambda_{res}$ is the defect mode wavelength at two different temperatures, ΔT is the temperature difference. The room temperature is used as a reference temperature to calculate $\Delta\lambda_{res}$ and ΔT. The signal-to-noise ratio (SNR), detection limit (δT), sensor resolution (SR), and figure of merits (FOM) are calculated from the following expressions

$$SNR = \frac{\Delta\lambda_{res}}{\Delta\lambda_{1/2}} \tag{22a}$$

$$\delta T = \frac{1}{S}\frac{\Delta\lambda_{1/2}}{1.5\,(SNR)^{0.25}} \tag{22b}$$

$$SR = \delta T\, S \tag{22c}$$

$$FOM = \frac{S}{\Delta\lambda_{1/2}} \tag{22d}$$

where, $\Delta\lambda_{1/2}$ is the full width at half maximum (FWHM) of the defect mode dip.

In Table 2, we calculated the structure parameters at d_{TiO_2} = 62.5 nm because as was seen the sharpness of the defect modes in Fig. 3(a) is better than in Fig. 3(b). So, we expected that the defect thickness of the quarter wavelength will produce high performance for the structure design. The results in Table 2 show that our

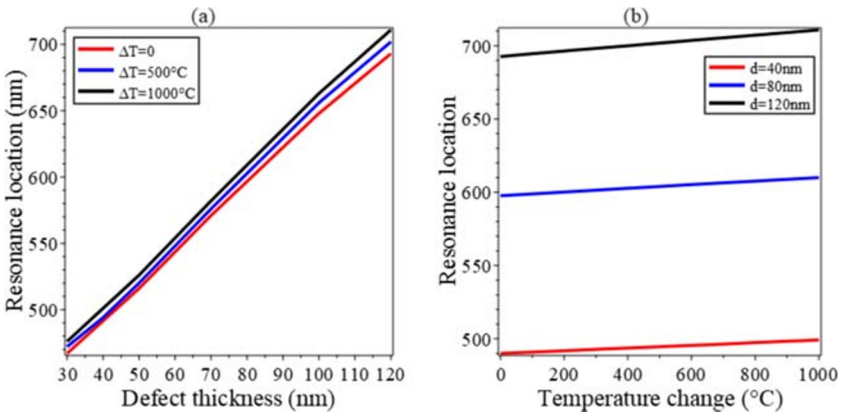

Fig. 4 The resonance location in the $[(Si/SiO_2)^5\ TiO_2\ (Si/SiO_2)^5]$ APC versus (a) different thicknesses of the defect TiO_2 layer at three different temperatures and (b) Temperature changes at three thicknesses of the defect TiO_2 layer.

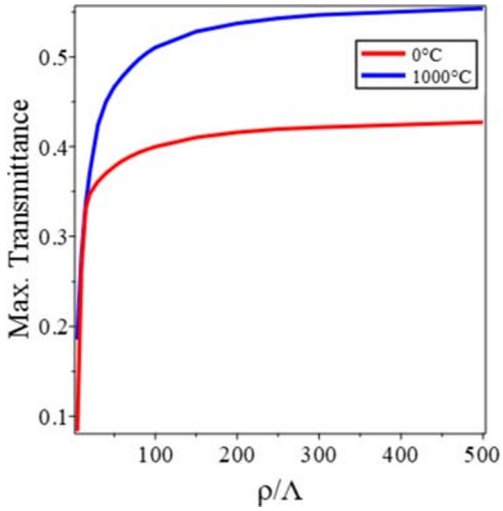

Fig. 5 The maximum achievable transmittance versus the core radius (normalized to the period Λ) for ΔT = 0 °C (red) and ΔT = 1000 °C (blue). The number of periods N = 10 and the defect layer thickness d_{TiO_2} = 62.5 nm.

proposed defective APCs temperature sensor has good results for all performance parameters. The resonant wavelength increases with increasing temperature while the sensitivity decreases because the ratio of temperature increase is higher than the ratio of resonant wavelength increase. The other factors also increase as temperature increases. The decrease in $\Delta\lambda_{1/2}$ with temperature means that the defect mode gets sharpened with increasing temperature. This is an important parameter in studying sensor quality. FOM and SNR also increase with temperature change. The detect limit δT and sensor resolution SR decrease with temperature changes and the structure becomes more sensitive. In fact, previous studies have achieved higher sensitivity than our design. For example, Tong et al. introduced Si / SiO_2 PCs temperature sensor with a sensitivity of the value 26 nm / 1000 °C [42] but they depend on the variation on the width of the PBG with no other performance parameters. Arun Kumar et al. introduced one dimensional PCs sensor with a sensitivity of about 0.064 nm / °C but with small FOM and high FWHM [43]. Also, Qiang Liu et al. studied a compact PC fiber as a temperature sensor with high sensitivity of 1.85 nm / °C but with very small FOM 0.072 / °C [44].

In Table 3, we calculated the previous performance parameters based on the variation of the defect layer thickness at a specific temperature of 1000 °C. From the first glance at the table, one can see that the sensitivity increases with temperature change in good consistency with the prediction from Fig. 3(a) above. Another interesting point is the close results for the thickness value of 60 nm in this table and the results of d_{TiO_2} = 62.5 in Table 2 at 1000 °C (the two highlighted rows in both tables).

4 Conclusion

In conclusion, we studied the thermal properties of the one dimensional defective APCs based on the transfer matrix method in the cylindrical coordinates. The transmission spectrum of our defective APCs is plotted versus temperature changes in the visible region. The temperature dependence of the defect mode in the defective APC is investigated and discussed. The defect mode location is plotted versus different temperatures and the defect layer thickness as well. The results revealed that the proposed temperature sensor showed a sensitivity of about 11 nm / 1000 °C, figure of merit of 0.218 / ^{0}C and a very small full width at half maximum of about 0.049 nm. We could achieve a high-performance temperature sensor which may play an effective role in many optical and communication applications. In view of the comparatively high sensing performance, APCs can take the role of traditional 2D and 3D planar PC sensors. They offer both ease in fabrication and high performance. The proposed sensor design could present a new novel method to overcome the limited performance of other temperature PC sensors. This response may attract the attention of many researchers who are of interest at the thermal properties of PCs from the design and the fabrication views.

Table 2 Some performance parameters of the proposed APCs at different temperatures (d_{TiO_2} = 62.5 nm)

ΔT (°C)	$\Delta\lambda_{res}$ (nm)	S (nm°C^{-1})	$\Delta\lambda_{1/2}$ (nm)	SNR	FOM (°C)	δT (°C)	SR (nm)
200	2.18	0.01090	0.070	31.14	0.156	1.812	0.0198
400	4.35	0.01087	0.064	67.94	0.170	1.367	0.0149
600	6.49	0.01082	0.063	103.08	0.172	1.218	0.0132
800	8.61	0.01076	0.060	143.43	0.179	1.074	0.0116
1000	**10.69**	**0.01069**	**0.049**	**218.20**	**0.218**	**0.795**	**0.0085**

Table 3 Some performance parameters of the proposed APCs for different defect thicknesses at a specific temperature = 1000° C

h_d (nm)	$\Delta\lambda_{res}$ (nm)	S (nm°C^{-1})	$\Delta\lambda_{1/2}$ (nm)	SNR	FOM (°C)	δT(°C)	SR (nm)
40	9.18	0.00918	0.090	102	0.102	2.06	0.019
60	**10.58**	**0.01069**	**0.056**	**189**	**0.189**	**0.95**	**0.010**
80	12.01	0.01201	0.070	172	0.171	1.07	0.013
100	15.23	0.01523	0.135	113	0.113	1.81	0.028
120	17.72	0.01772	0.322	55	0.055	4.45	0.079

Compliance with Ethical Standards

Conflict of Interest Authors declare that there are no conflicts of interest.

References

1. Elsayed HAE, Abadla MM (2019) Transmission investigation of one-dimensional Fibonacci-based quasi-periodic photonic crystals including nanocomposite material and plasma. Phys Scr 95: 035504. https://doi.org/10.1088/1402-4896/ab4c68
2. Abadla MM, Tabaza NA, Tabaza W, Ramanujam NR, Joseph Wilson KS, Vigneswaran D, Taya SA (2019) Properties of ternary photonic crystal consisting of dielectric/plasma/dielectric as a lattice period. Optik 185:784–793
3. Devashish D, Ojambati OS, Hasan SB, van der Vegt JJW, Vos WL (2019) Three-dimensional photonic band gap cavity with finite support: enhanced energy density and optical absorption. Phys Rev B 99:075112
4. Ahmed AM, Mehaney A (2019) Ultra-high sensitive 1D porous silicon photonic crystal sensor based on the coupling of Tamm/Fano resonances in the mid-infrared region. Sci Rep 9:6973
5. Elsayed HA, Mehaney A (2019) A new method for glucose detection using the one dimensional defective photonic crystals. Mater Res Express 6:036201
6. Elsayed HA (2018) A multi-channel optical filter by means of one dimensional n doped semiconductor dielectric photonic crystals. Mater Chem Phys 216:191–196
7. Abd El-Aziz OA, Elsayed HA, Sayed MI (2019) One-dimensional defective photonic crystals for the sensing and detection of protein. Appl Opt 58(30):8309–8315
8. Yang S, Zhang Y, Peng X, Lu Y, Xie S, Li J, Chen W, Jiang Z, Peng J, Li H (2006) Theoretical study and experimental fabrication of high negative dispersion photonic crystal fiber with large area mode field, opt. Express 14(7):3015–3023
9. Yablonovitch E (1987) Inhibited spontaneous emission in solid-state physics and electronics. Phys Rev Lett 58:2059–2062
10. John S (1987) Strong localization of photons in certain disordered dielectric Superlattices. Phys Rev Lett 58:2486–2489
11. El-Naggar SA (2015) Tunable terahertz omnidirectional photonic gap in one dimensional graphene-based photonic crystals. Opt Quant Electron 47:1627–1636
12. Aly AH, Mohamed D, Elsayed HA, Mehaney A (2018) Fano resonance by means of the one-dimensional superconductor photonic crystals. J Supercond Nov Magn 31(12):3827–3833
13. Notomi M, Shinya A, Mitsugi S, Kira G, Kuramochi E, Tanabe T (2005) Optical bistable switching action of Si high-Q photonic-crystal nanocavities. Opt Express 13:2678–2687
14. Hadfield RH (2009) Single-photon detectors for optical quantum information applications. Nat Photon 3:696–705
15. Aly AH, Elsayed HA (2017) Tunability of defective one dimensional photonic crystals based on faraday effect. J Mod Opt 64(419):871–877
16. Segovia-Chaves F, Vinck-Posada H (2019) Tuning of the defect mode in a 1D superconductor-semiconductor crystal with hydrostatic pressure dependent frequency of the transverse optical phonons. Physica C 556:7–13
17. Segovia-Chaves F, Vinck-Posada H, Dhasarathan V, Rajan MSM (2019) Transmittance spectrum in a 1D photonic crystal composed fused silica and sea water. Optik 185:930–935
18. Chen T, Han Z, Liu J, Hong Z (2014) Terahertz gas sensing based on a simple one-dimensional photonic crystal cavity with high-quality factors. Appl Opt 53:3454–3458
19. Wu J, Gao J (2015) Low temperature sensor based on one-dimensional photonic crystals with a dielectric-superconducting pair defect. Optik 126:5368–5371
20. Elmahdy, N A, Esmail, M S & El-Okr, M M (2018). Characterization of a thermal sensor based on one-dimensional photonic crystal with central liquid crystal defect, Optik, 170, 444–451
21. Srivastava SK, Aghajamali A (2016) Investigation of reflectance properties in 1D ternary annular photonic crystal containing semiconductor and high-T c superconductor. J Supercond Nov Magn 29(6):1423–1431
22. Kaliteevski MA, Abram RA, Nikolaev VV, Sokolovski GS (1999) Bragg reflectors for cylindrical waves. J Mod Opt 46(5):875–890
23. Hu C-A, Wu C-J, Yang T-J, Yang S-L (2013) Analysis of optical properties in cylindrical dielectric photonic crystal, opt. Communications 291:424–434
24. Hu C-A, Wu, Yang S-L, Yang T-J (2013) Switchable tunneling mode for cylindrical photonic quantum well consisting of photonic crystals containing liquid crystal. Opt. Communications 297:141–146
25. Srivastava SK, Aghajamali A (2016) Study of optical reflectance properties in 1D annular photonic crystal containing double negative (DNG) metamaterials. Physica B 489:67–72
26. Chen M-S, Wu C-J, Yang T-J (2012) Narrowband reflection-and-transmission filter in an annular defective photonic crystal containing an ultrathin metallic film, opt. Communications 285:3143–3149
27. El-Naggar SA (2019) Properties of defect modes in cylindrical photonic crystals. Optik 200:163447
28. Chang Y-H, Jhu Y-Y, Wu C-J (2012) Temperature dependence of defect mode in a defective photonic crystal, opt. Communications 285(6):1501–1504
29. Nikolaev VV, Sokolovskii GS, Kaliteevskii MA (1999) Bragg reflectors for cylindrical waves. Semiconductors 33(2):147–152
30. Elsayed HA, El-Naggar SA, Aly AH (2014) Thermal properties and two-dimensional photonic band gaps. J Mod Opt 61(5):385–389
31. Cheng, D K (1983). Field and wave electromagnetics, Addison Wesley Publishing Company, Canada

32. Chourasia RK, Yadav CS, Upadhyay A, Chourasia NK, Singh V (2020) Analysis of Bragg fiber waveguides having a defect layer for biosensing applications. Optik 200:163400
33. Chen M-S, Wu C-J, Yang T-J (2009) Optical properties of a superconducting annular periodic multilayer structure. Solid State Commun 149:1888–1893
34. Pedrotti, F L Pedrotti, L M & Pedrotti, L S (2007). Introduction to optics, Pearson Prentice Education Inc., New Jersey
35. Tatian B (1984) Fitting refractive-index data with the Sellmeier dispersion formula. Appl Opt 23(24):4477–4485
36. Wiechmann S, Müller J (2009) Thermo-optic properties of TiO2, Ta2O5 and Al2O3 thin films for integrated optics on silicon. Thin Solid Films 517(24):6847–6849
37. Singh SP, Pal K, Tarafder A, Das M, Annapurna K, Karmakar B (2010) Effects of SiO2 and TiO2 fillers on thermal and dielectric properties of eco-friendly bismuth glass microcomposites of plasma display panels. Bull Mater Sci 33(1):33–41
38. Ye, W N, Sun, R, Michel, J, Eldada, L, Pant D & Kimerling, L C (2008). 5th IEEE international conference on group IV photonics, Sorrento, Italy, 401
39. Iliew R, Etrich C, Pertsch T, Lederer F, Staliunas K (2008) Subdiffractive all-photonic crystal Fabry-Perot resonators, opt. Letters 33(22):2695
40. El-Khozondar HJ, Shabat MM, Abu Tair G, Abadla M (2007) Thermal-stress effects on nonlinear thin film waveguide sensors. J Phys Chem Solids 8(2):260–264
41. Mehaney A (2019) Biodiesel physical properties detection using one-dimensional Phononic crystal sensor. Acoust Phys 65(4): 374–378
42. Tong K, Cui W, Yan G, Li Z (2007) Study on temperature property of band structures in one-dimensional photonic crystals. Optoelectr Lett 3(6):444–447
43. Kumar, A, Kumar, V, Suthar, B, Bhargava, A, Singh, K S, & Ojha, S P (2012). Wide range temperature sensors based on one-dimensional photonic crystal with a single defect, Int J Microw Sci Techn, 1–5
44. Liu Q, Li S, Chen H, Fan Z, Li J (2015) Photonic crystal Fiber temperature sensor based on coupling between liquid-Core mode and defect mode. IEEE Photon J 7(2):1–9